PERGAMON

Engineering Fracture Mechanics 63 (1999) 395-411

www .elsevier .com/locate/engfracmech

In-situ observation of damage evolution and fracture in AlSi7MgO.3 cast alloys

L.L. Mishnaevsky Jr [a,b,*], N. Lippmann [c], S. Schmauder[b], P. Gumbsch[a]

[a] *Max-Planck-Institut für Metallforschung, Seestr.* 92,70174 *Stuttgart, Germany*
[b] *Staatliche Materialprüfungsanstalt (MPA), University of Stuttgart, Pfaffenwaldring* 32,70569 *Stuttgart, Germany*
[c] *Robert Boscli GmbH, FV/PLM, PO Box* 300240, 70442 *Stuttgart, Germany*

Received 16 January 1998; accepted 10 February 1999

Abstract

The mechanisms which occur during damage initiation, evolution and crack growth in A1Si7MgO.3 cast alloys are studied by in-situ tensile testing in a scanning electron microscope. It is shown that microcracks in these alloys are predominantly formed in the Si particles. Shear bands are seen to precede the breaking of the Si particles and the dislocation pile-up mechanism can thus be confirmed as the dominant damage initiating process in the matrix. Both micro- and macrocrack coalescence have been observed in the course of the experiments. The effect of the microstructure of the A1Si7Mg cast alloys on damage nucleation, crack formation and compliance reduction is analysed.

1. Introduction

A1Si7Mg cast alloys are now widely used as structural materials in industry and their production increased remarkably during the last years [1]. The practical application of these materials is based on their strength and fracture resistance. To further improve the strength of the material, it is necessary to have a good understanding of the damage evolution and fracture of these alloys. The purpose of the paper is to clarify the mechanisms of damage initiation, damage evolution, compliance reduction and fracture of two A1Si7Mg cast 0.3 alloys with almost identical composition but very different microstructure.

Corresponding author. Te1.: + 49- 711-685-3049; fax: + 49- 711-685-2635.
E-mail address: impgmish@mpa.uni-stuttgart.de (L.L. Mishnaevsky *Ir)*

0013-7944/99/$ -see front matter (!;;) 1999 EIsevier 8cience Ltd. All rights reserved. PII: 80013-7944(99)00027 –2

Several investigations of the failure of A1Si cast alloys have been reported in the literature. Gurland and Plateau [2] studied the ductile rupture of an A1Si13 alloy and obtained an expression for the particle cracking stress and a relation between fracture strain and the fraction of broken particles. Yeh and Liu [3] have studied the cracking of silicon particles in

aged A1Si7Mg (A357) alloys. They analysed the mechanism responsible for the cracking of the Si particles and the effects of strain and stress on the fraction of broken Si particles. Yeh and Liu have shown that the dislocation pile-up mechanism is the most probable one among other theories of the failure of Si-particles. Höner and Groß [1] studied the fracture behaviour and tensile strength of A1Si alloys and its dependence on the microstructure, which is determined in turn by the conditions of melt processing and casting.

The outline of this paper is as follows: in section 2 we briefly discuss the mechanisms and models of crack initiation and crack growth in ductile materials. Section 3 gives a description of the experimental details. An analysis and discussion of our results is given thereafter .

2. Failure mechanisms of ductile materials

The course of failure in ductile materials is generally divided into three stages [1,4-6]:

1. Nuc1eation of microcracks/microvoids at random positions in the loaded body independent of their location relative to the other microcracks. The growth rate of the microcrack density usually increases with increasing density of microcracks [7]. This nucleation stage is followed by:
2. The link-up and coalescence of microcracks and the formation of the 'macro-cracks', which leads to:
3. The growth of the macrocracks until one of the cracks reaches a critical size and begins to grow autocatalytically. This finally results in the complete failure of the body.

All these processes proceed not only successively, but also simultaneously. For instance, growth of a crack can proceed simultaneously with the increase in the microcrack density.

2.1. *Microcrack nucleation*

The mechanisms of microcrack initiation are discussed in detail by Knott [8] and Tetelman and McEvily [4]. Tetelman and McEvily have shown that large tensile stresses as well as shear stresses develop at the tip of a glide band if the band is blocked by a strong obstacle. They determined the conditions of crack nucleation, and showed that the tensile stresses are less important during the nucleation process than the shear stresses. Knott [8] described and analysed several micro-mechanisms of fracture. Among them are microcrack nucleation by squeezing together of dislocations at the head of the slip band (Stroh model) or by the interaction of a pile-up with a carbide particle (Smith model). The model developed by Yeh and Liu to describe the failure of Si-particles ii1 their A1Si7Mg alloys is similar to the Smith model and explains the microcrack initiation as a result of particle failure caused by stress concentrations originating from dislocation pile-ups at these particles.

2.2. Void and microcrack coalescence

Thomason [9] describes void coalescence with a mathematical model for the coalescence of square holes arranged into a square array in a rigid-plastic matrix under tension. The voids are elongating in the direction of the tensile load and approach each other in the direction normal to the tensile load. When the voids get close, necking OCCU!S between them and they coalesce rapidly. The deformation of the material between the voids therefore controls void coalescence and necking. Finkel [5] has studied experimentally the necking between microcracks. He showed that the failure of the necks between microcracks is caused by shear stresses. Seidenfuss [10] recognised three possible mechanisms of void coalescence: local plastic constriction of material between voids, failure of the layer between voids caused by shear bands and failure by formation of secondary smaller voids on very small inclusions in the material between available voids. He noted that the joining of voids proceeds in a stepwise manner. The first mechanism dominates when the density of voids is high, the third prevails at relatively low void densities. Seidenfuss concluded that the main mechanism of void coalescence is the formation of shear bands in which small secondary voids can sometimes be observed. Shear bands causing the failure of the layers between coalescing voids have also been observed by Roberts et al. [11]. With regard to the interaction of macrocracks, it is known that: 'originally collinear mode I cracks seem to avoid each other' [12]. On the basis of the analysis of the stability of straight crack paths, Melin has shown that the tip to tip coalescence of cracks does not occur for two collinear cracks [12].

2.3. *Formation and growth of macrocracks*

Crack growth as a result of the superposition of stress fields from a large crack and from a pile- Up of dislocations in the vicinity of the crack tip has been modeled by Yokobori [13]. In this model the dislocation pile-up acts as a stress concentrator similar to a microcrack. The stress required for macrocrack growth is much higher than the stress required for microcrack formation from a pile-up of dislocations. As a consequence, ductile fracture is usually determined by the formation of a microcrack in the vicinity of a large crack, and not by crack growth itself. Ebrahimi and Seo [14] have shown that crack propagation in ductile materials may also involve the cleavage of favourably oriented grains ahead of the main crack tip followed by ductile tearing of remaining ligaments. The formation of river patterns on the fracture surface has been attributed [4] to the joining of the main crack with secondary new cracks nucleated ahead of the main crack. Joining can occur by tearing (tongue formation) or secondary cleavage.

From the above considerations, it follows that although the main models of fracture are based on the assumption that the crack grows in a continuous material (or, as a version, in continuous material with a plastic zone in the vicinity of the crack tip) [8], the real physical mechanisms of fracture can differ significantly from this assumption.

3. Experimental procedure

The course of damage evolution in AISi7Mg cast alloys was observed by in-situ tensile testing in a scanning electron microscope (SEM). Fig. 1 gives the geometry and the dimensions

of the notched C T -specimens used in our experiments. The notches in the specimens were sawn with a saw blade with a defined radius of the saw teeth equal to the required radius of the notch. Such notching ensures high quality of the notch surface. The side surface of the C T - specimens was ground and subsequently polished with diamond paste down to the 3 ~m grade. The specimens were taken from cast components.

The heat treatment of the components included a solution annealing in an air circulation kiln for 12 h at 540°C and the artificial ageing in an air circulation kiln for 12 h at 170°C.

The specimens were loaded in an in-situ tensile stage (Fa. Raith, Dortmund, Germany) in

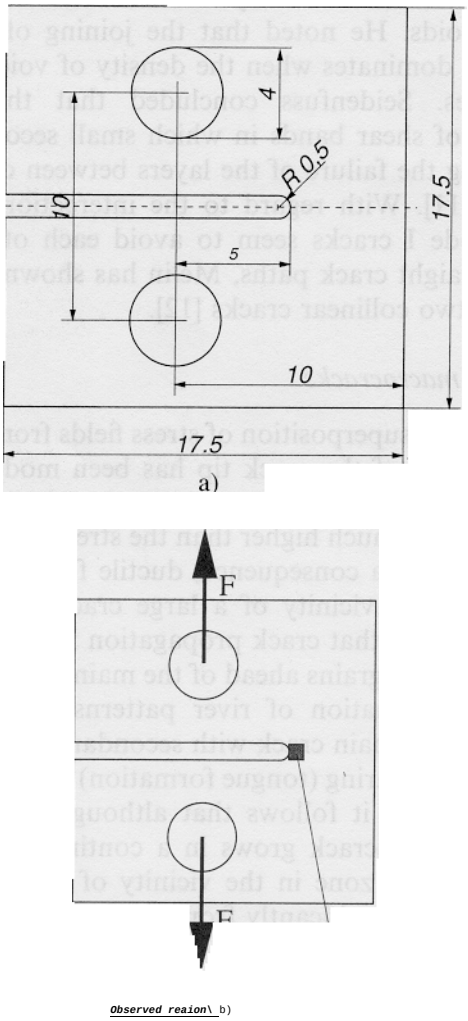

Fig. 1. Shape and size of the CT-specimen (a) and the small area in the notch root (b) which was observed during the tests. Dimensions are given in mm.

the SEM. A constant crosshead speed or 0.3 ~m/s was used. The specimens were loaded until a large crack was visible on the surface or the specimens. During loading, the highly deformed region in the notch root (about 100 x 100 ~m) or the C T -specimens was monitored.

The experiments were conducted on AISi cast alloys or the type A1Si7MgO.3 with both lamellar and globular microstructure or the Si-particles. In the lamellar structure, the Si

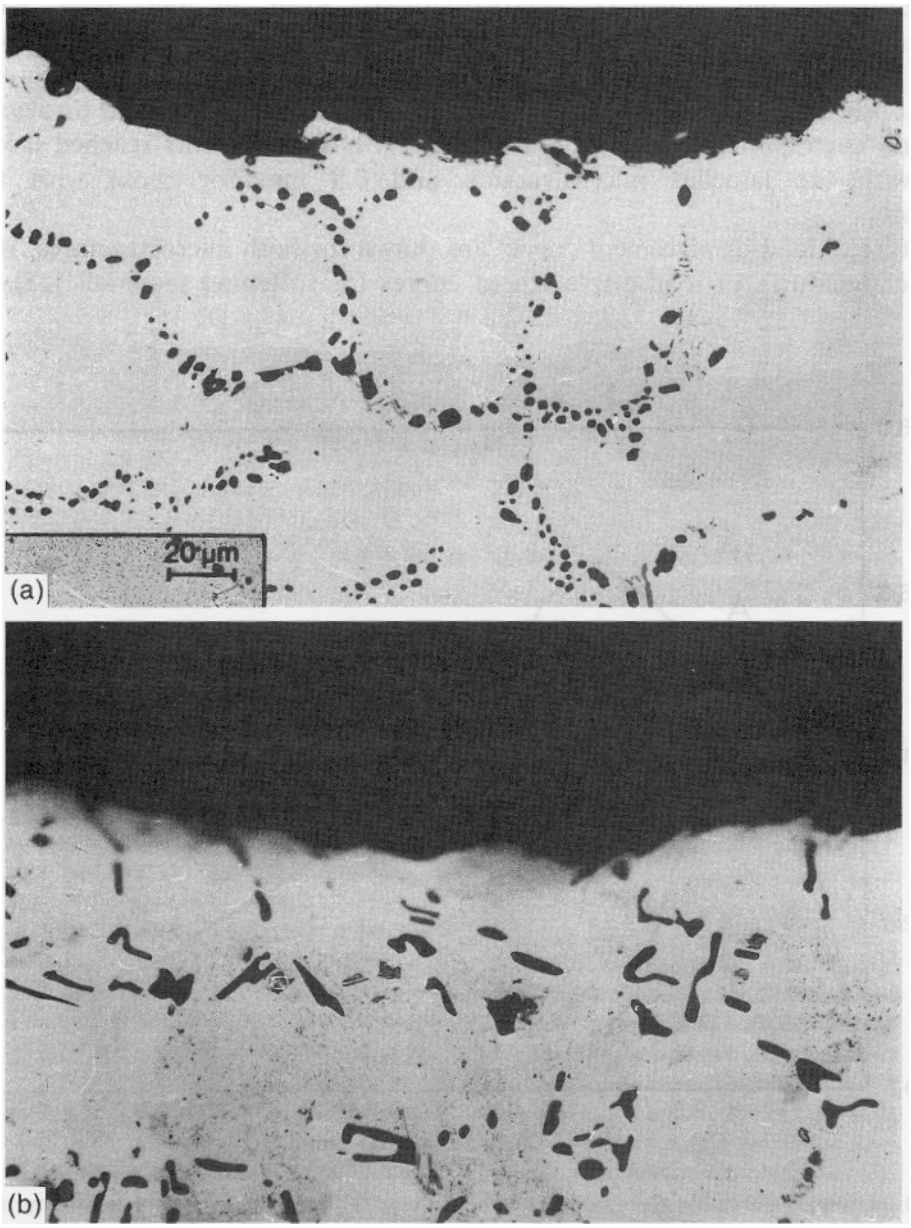

Fig. 2. Micrographs of the two microstructures: Ca) globular and Cb) lamellar Ca scale is the same).

inclusions had an aspect ratio (length to width) of about 4...20 and the small dimension of the particles was between 2.5 and 5 μm. The Si particles can be transformed into a more rounded shape by the addition of Sb. The particles in the globular microstructure were approximately circular with a diameter of about 3-6 μm. The diameter of the Al grains was between 50 and 130 μm. The Si-particles in the alloys were located preferentially (but not exclusively) on the Al grain boundaries corresponding to the fact that the growth of Al grains during the formation of the alloy is inhibited by the available Si-particles. Fig. 2 shows micrographs of the two different (globular and lamellar) microstructures. Even in the alloy with globular microstructure the Si-particles form a network and each cell of the network corresponds to a grain of the Al-matrix.

Simultaneously with the loading of the specimens, the externally applied displacement of the crosshead and corresponding load were recorded. The displacements reached 0.5 mm for the specimens with the lamellar microstructure and 0.9 mm for those with the globular microstructure.

In Fig. 3 typical load-displacement curves are shown for both microstructures. Both have the characteristic signatures of load-displacement curves for softening materials [15]. At first, the

applied force increases almost linearly with increasing displacement and then reaches a peak. The following decease was most pronounced in the alloy with lamellar microstructure. The macrocracks formed later and grew when the curve was already descending considerably. These processes will be detailed in the following section.

4. Microcrack initiation and evolution

At the initial stages of loading, the formation of shear bands was observed in the ground notch region near the surface. Then, several microcracks appeared at some distance from the notch surface. This stage is indicated with label A in Fig. 3 and corresponds to the displacement of 0.13 and 0.16 mm for the alloys with lamellar and globular structures, respectively. The applied force was approximately 500 N for both microstructures.

The microcracks initiated exclusively in the Si-particles. The amount of broken Si-particles in relation to the total number of particles in the observed area of the alloy with lamellar structure was about 4%. A similar calculation for the globular structure was not possible since the cluster arrangement of the Si-particles on the boundaries of the Al-grains did not allow to distinguish individual broken particles. Thereafter, additional matrix shear bands formed and the density of microcracks increased.

Figs. 4 and 5 show the microcracks formed at the initial stage of damage evolution. The

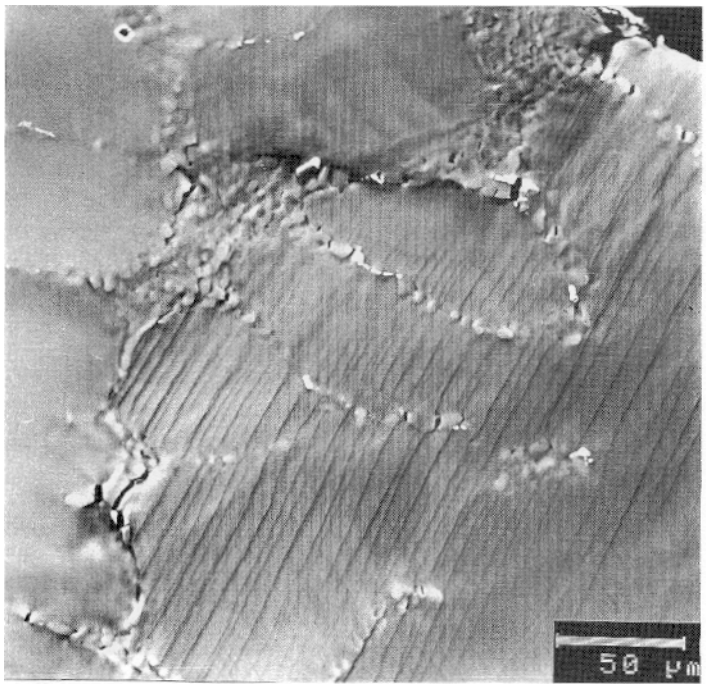

Fig. 4. Area in the vicinity of the notch root (globular microstructure; magnification x350; displacement 0.185 mm).

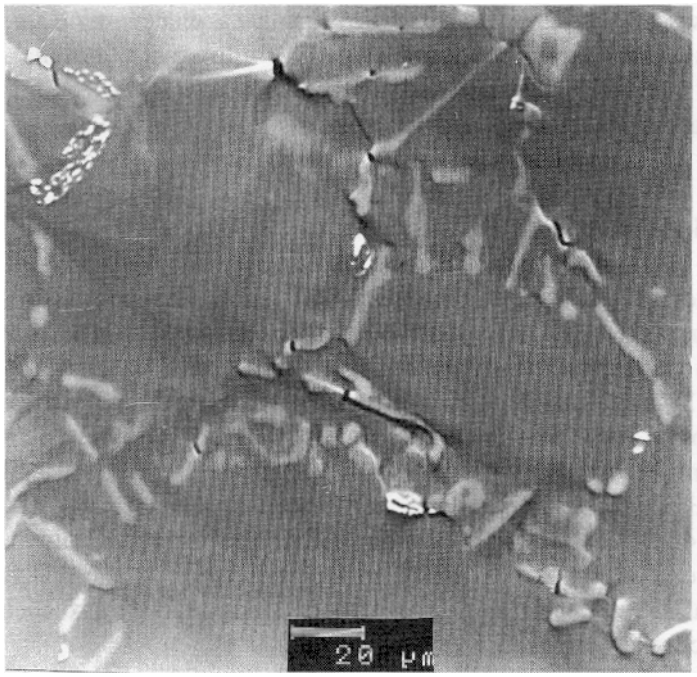

Fig. 5. Area in the vicinity of the notch root (lamellar microstructure; magnification x500; displacement 0.16 mm).

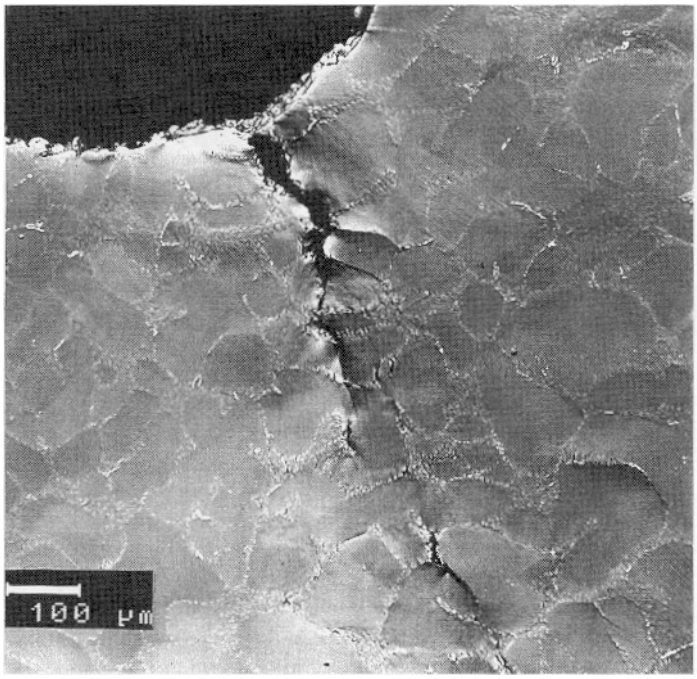

Fig. 6. Crack formation in the vicinity of notch root and crack initiation at some distance from the notch root (globular microstructure; magnification x 100; displacement 0.55 mm).

micrographs represent small areas rather close to the notch surface, and correspond to the alloys with the globular and lamellar microstructure, respectively. The microcracks are more or less randomly distributed up to a distance of about 300 !lm from the notch surface (0.6 notch radii). The microcracks thus are oriented mostly along the lines of maximum shear stress. Upon further increasing the applied load, the nucleation and accumulation of microcracks at some distance from the notch is accompanied by nucleation and growth of cracks from the notch surface.

In summary, during the initial stages of damage evolution in the AlSi7Mg cast alloys the destruction of the Si-particles was the prevailing mechanism of microcrack nucleation. Microcracks formed predominantly at 'random' sites throughout the stressed area and not at the root of the notch.

5. Crack growth and coalescence

At the next stage of damage evolution, relatively large cracks formed from initially small surface cracks. Simultaneously, the density of microcracks at some distance from the notch surface increased and several small cracks formed there. Figs. 6 and 7 show the large crack which starts at the notch surface and the smaller cracks and microcracks formed at some distance from the notch surface. The micrographs shown on Figs. 6 and 7 correspond to the points marked with the letter B on the force-displacement curve (Fig. 3).

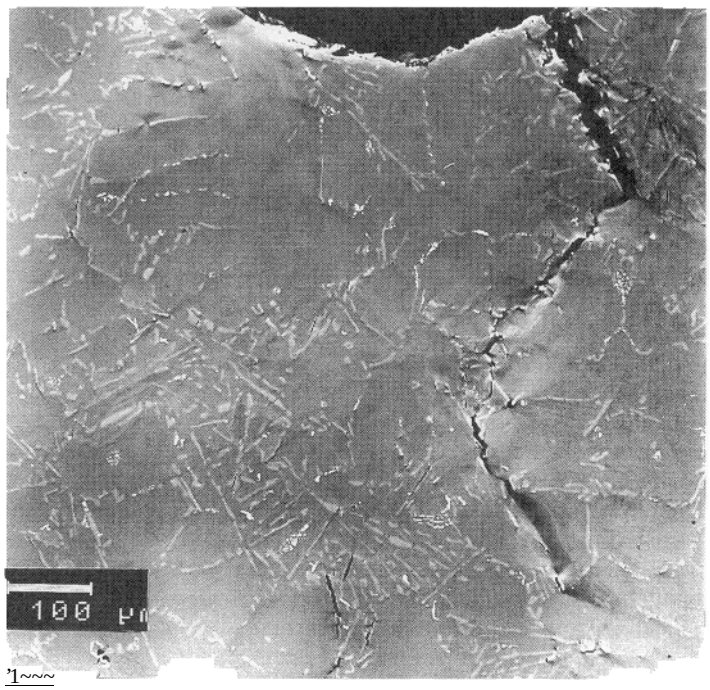

Fig. 7. Crack formation in the vicinity of notch ground (lamellar microstructure). The microcracks set the crack path (magnification x 115; displacement 0.20 mm),

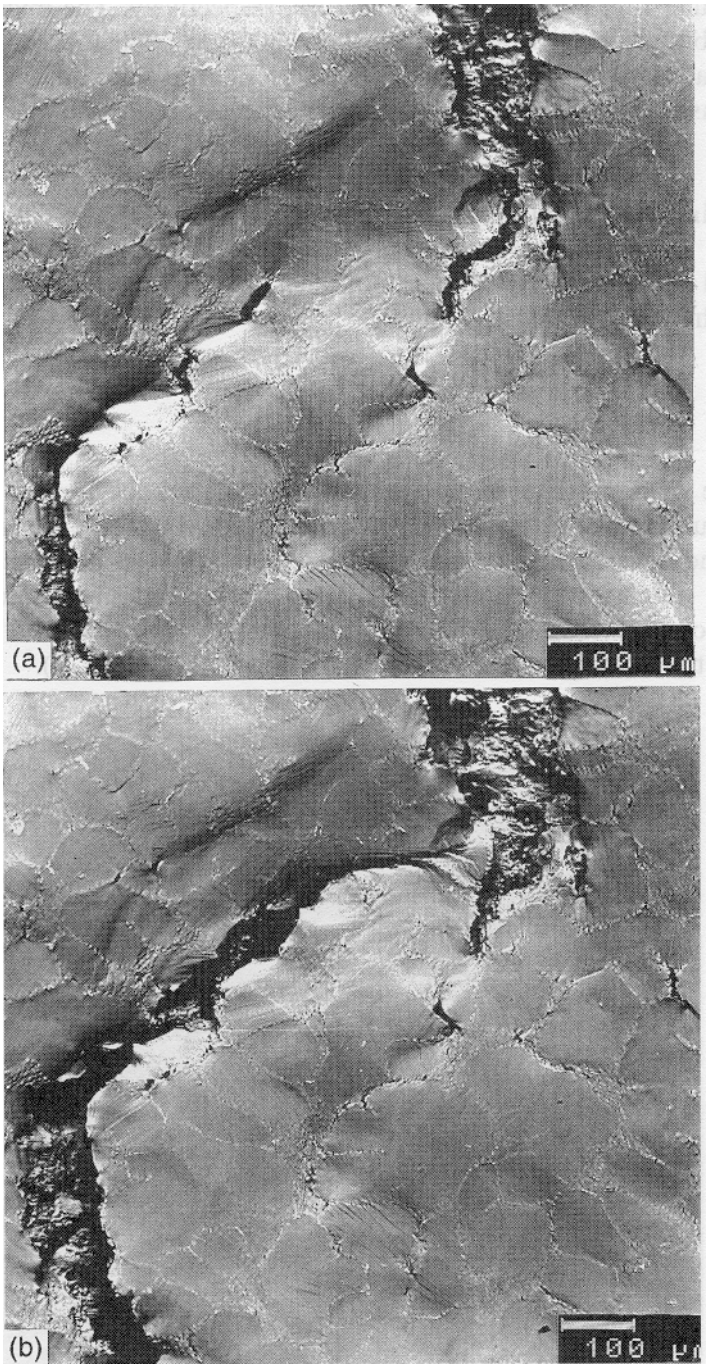

Fig. 8. Crack coalescence in the alloy with globular microstructure. Two cracks (a) before and (b) after coalescence (magnification x 100; displacement (a) 0.76 and (b) 0.89 mm).

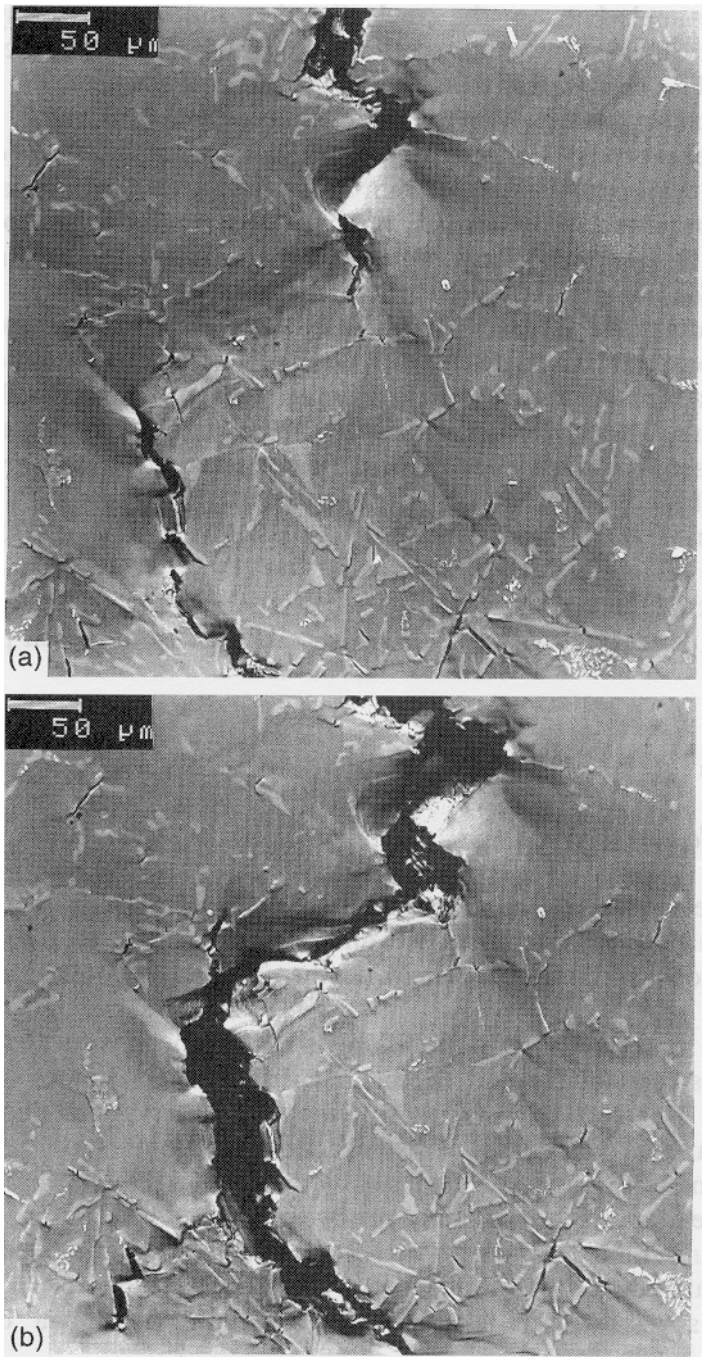

Fig. 9. Crack coalescence in the alloy with lamellar microstructure. Two cracks (a) before and (b) after coalescence (magnification x200; displacement (a) 0.35 and (b) 0.43 mm).

Comparing Figs. 6 and 7, it is seen that the direction of the cracks is the same for both microstructures. The angle between the crack direction and the axis of symmetry of the CT - specimen was about 30°. Shear bands are apparent between the large cracks and the small cracks (cf. Fig. 7). The large crack then grew and joined with the small cracks in front. The path of the large crack corresponds to the direction from the crack tip to the available microcracks and shear bands. The small cracks and microcracks then joined and formed a second large crack located about 0.4-0.5 mm away from the notch surface (about 0.9 notch radii). The formation of the second large crack was observed at a load point displacement of about 0.24 mm and at an applied force of 100 N for the lamellar microstructure and at about 0.7 mm and 180 N for the globular microstructure.

Upon further loading, the large crack from the notch surface and the second crack join. Figs. 8 and 9 show this coalescence for the globular and the lamellar microstructure, respectively. Figs. 8a and 9a depict the earlier stages when there are still two separate large cracks in the materials. This stage corresponds to the points marked with the letter C in Fig. 3. Figs. 8b and 9b present the later stage when the cracks coalesced and formed one single large crack, labeled with the letter D in Fig. 3.

It is of interest to note that almost the same crack patterns formed in both materials, although the structures of the materials differ significantly. The crack paths followed the location of the microcracks in front of the tip only until a second large crack was available at close distance. Then the interaction between the stress fields of the cracks determined their paths.

6. Analysis of results

6.1. Microcrack nucleation

The prevailing mechanisms of microcrack initiation in the AlSi7Mg cast alloys investigated in this study can be clarified by comparison and correlation with the results of other authors. The first step is to identify the mechanisms and the criteria controlling the breaking of the Si- particles.

One may assume that the Si-particle failure is caused by a critical level of the maximal tensile stress. In this case, one would expect that the first microcracks initiate directly at the center of the notch. This is clearly inconsistent with our observations that the microcracks are formed mostly in random sites at some distance from the notch surface. Therefore, it follows that local fluctuations of the stress field caused by dislocation pile-ups and Si-particles influence the microcrack nucleation much more than the overall stress distribution.

Following Yeh and Liu [3], the critical length of a dislocation pile-up which causes the breaking of the particles can be calculated. They derived the following formula for the externally applied stress (1e required for particle failure due to a one-plane pile-up of dislocations:

$$\sigma_e = \sqrt{\frac{EGb}{2(1-\nu)LM^2\pi^2}}$$

where E is the Young's modulus, G is the shear modulus, b is the Burgers vector, v is the Poisson ratio, M is the Schmid factor and L is the length of the pile-up. In our experiments, the first broken Si-particles were observed in the notch region at an externally applied load of about 500 N (see Figs. 4 and 5). At this load the Al matrix in the notch ground starts yielding, which for this specific matrix alloy has been shown to begin at 218 MPa [16]. Taking the angle at which particle cracking first occurs from the micrographs (Figs. 4,5; () ~ 30°), one calculates a Schmid factor of

$$M = \sin\theta \cos\theta \sim 0.43. \tag{2}$$

Substituting the values E= 100 GPa, v=0.33, G=40 GPa [3], b=0.286 nm [17] and the local stress (σe=218 MPa into Eq. (1), one obtains: L=9.9 μm. This value is rather close to the pile- up length calculated by Yeh and Liu for the as-quenched conditions (L= 14.4 μm [3]). This length corresponds to

$$n = \frac{(1-\nu)\pi\tau L}{Gb} \tag{3}$$

dislocations in the pile-up, where τ -shear stress. If τ is again taken to be of the order of the yield stress (218 MPa), Eq. (3) gives n ~ 250 dislocations in the pile-up. Our results differ here from the results of Yeh and Liu, who have used the value of the external stress (17.2 MPa). Since our in-situ observations show that the aluminum matrix already deformed plastically we claim that the local stress level must be larger than the externally applied stress and of the order of the yield stress of the matrix. This value for the length of the pile-up is very reasonable since it is about 5-10 times lower than the linear size of Al-grains.

Together with the direct observation that the microcracks are located mostly along the lines of maximum shear stress and always appear together with the first shear bands, our data strongly support the dislocation pile-up mechanism as the origin of particle failure.

Our in-situ observations (Figs. 4 and 5) linked with the load-displacement diagram (Fig. 3) confirm that the microcracks are responsible for the compliance reduction of the material. It is apparent that the microcracks are formed just before the peak load is reached and macroscopic compliance reduction starts after the density of microcracks reached a reasonable value. The rate at which the compliance reduction proceeds, however, is determined by the microcrack coalescence.

6.2. *Crack growth and coalescence*

The formation of (small) cracks through the coalescence of microcracks as described above complies rather with the descriptions of microcrack coalescence given by Finkel [5], Seidenfuss [10] and Roberts et al. [11] than that by Thomason [9]. Microcrack coalescence was observed only after shear bands were formed between them, and not due to their expansion or growth.

It was also observed that the macrocracks are initiated on and propagate from the notch surface, although the microcracks are nucleated at some distance from the surface. Again, shear bands are responsible for the crack initiation there.

The final destruction of the material via the initiation and growth of the surface crack, the

formation of the second crack from random I y distributed microcracks at some distance from the surface and the coalescence of the macrocracks bears many similarities with the mechanisms described in the literature [5,14]. A few aspects, however, are very different: the microcracks in the material were not on I y formed in the vicinity of the crack tip as a result of the stress field from the crack, but also in 'random' sites throughout the stressed volume consistent with the dislocation pile-up model for their nucleation. Both microstructures showed the same behavior in this respect, which means that the following steps of damage evolution, the growth of the macrocracks and their coalescence, is determined by the global stress distribution in the loaded specimen (which is the same in both cases) rather than by the microstructure of the material.

In modelling the fracture processes in this alloy, one should therefore take into account not on I y microcracks which are formed in front of the growing crack and are absorbed by the crack, but also the distributed microcracks, which are formed simultaneously with the formation of the large crack and influence its path. The evolution of these distributed microcracks may lead to the formation of other large cracks, which interact with the existing ones.

6.3. Alloy microstructure, compliance reduction and fracture

Table I gives the consumed energies corresponding to the points marked on Fig. 3. The energy was calculated as the area under the curves of Fig. 3. Evidently, for the globular microstructure the energy needed to reach the descending .branch of the force-displacement curve is almost four times larger than for the lamellar structure.

Comparing Figs. 6 and 7 with the data from Table 1, ,the relation between the fracture energies of both alloys can be estimated, since the cracks in Figs. 6 and 7 are approximately of equal size. The energies differ by almost a factor of 4: 0.23 and 0.058 J, for globular and lamellar alloys, respectively. Therefore the energy needed to form the crack and to create a unit crack area of the alloy with the globular structure is about 4 times larger than that of the alloy with the lamellar structure.

The question now arises, what determines the differences in fracture characteristics (cf. Fig. 3) between the two different alloys investigated here and whether there is potential for

Table 1
Consumed energy J corresponding to the points marked on the force-displacement curves (Fig. 3)

Points on curves of Fig. 3	Lamellar microstructure	Globular microstructure
Appearance of first, randomly distributed microcracks (points A)	0.03	0.046
Peak load	0.042	0.119
Formation of a large crack (points B)	0.058	0.236
Formation of two large cracks (points C)	.083	0.292
Coalescence of large cracks (points D)	0.086	0.312

improvement. Up to this point many similarities between the two alloys have been discussed and no difference in failure mechanisms has been identified. Nevertheless, the descending branch in the load-displacement curves in Fig. 3 starts much earlier and compliance reduction is more pronounced in the alloy with the lamellar microstructure. The difference in reduction of stiffness of the material as a function of displacement is most pronounced at the initial stages of compliance reduction. In the lamellar structure, the load drops by a factor of ten when the displacement is increased from 0.15 to 0.3 mm. In contrast, the load only drops by a factor of 6 when the displacement is increased from 0.28 to 0.8 mm in the globular structure.

Having identified the necking along the shear bands formed between the microcracks as the main mechanism for their coalescence and the microcrack coalescence as the origin of the reduction of compliance, the different degree of the compliance reduction of the two alloys can be rationalized to some extent. The alloys differ mostly in the size of the Si-particles. The larger particles in the lamellar structure prohibit homogeneous slip transmittal and plastic deformation is concentrated on the few places at these particles where they are broken. This leads to less homogeneously distributed plastic deformation and microcrack distribution. A signature of this less even distribution is that the microcracks in the lamellar structure (Fig. 5) are opened much more clearly than those in the globular structure (Fig. 4) at similar strains. Consequently, the plastic strain in one individual slip band of the lamellar structure is significantly larger than in the globular structure and necking along these shear bands happens more readily.

The peak loads reached in the two alloys can be interpreted in a similar way. The peak load of the globular material is reached at a displacement which is approximately twice that of the lamellar material (0.281 and 0.144 mm, respectively). The peak load of the alloy with globular microstructure itself, however, is only 20% larger than that of the alloy with the lamellar structure (627 and 522 N, respectively). Again, if the coalescence of the microcracks is the decisive step for the compliance reduction and if coalescence is controlled by a critical plastic strain in the shear bands between the microcracks, the globular structure permits larger plastic strain since there are more paths for plastic deformation than in the lamellar structure and each of them has to carry comparatively less plastic strain. However, the corresponding stresses are only marginally higher since their level is mostly determined by the level at which yielding and microcrack initiation begin and this is similar for both alloys, irrespective of their microstructure.

Potential benefits for alloy development in this class of A1Si alloys are seen in two aspects, both are related to the microstructure refinement. Firstly, the reduction of the size of the Al- matrix grains should reduce the mean free path for dislocation pile-ups and might therefore prolong the initiation of the first microcracks to somewhat higher loads. Secondly, the size of the Si-particles and their shape should be pushed towards more rounded and more evenly distributed particles to avoid strain localization in shear bands and to prolong the compliance reduction of the material to higher total strains.

7. Conclusion

The course of crack initiation and growth in two AlSi7Mg cast alloys which are

distinguished by their globular and lamellar microstructure was investigated in-situ in a scanning electron microscope and can be described as follows:

- Nucleation of microcracks: microcracks are initiated predominantly by failure of Si-particles caused by dislocation pile-ups. This occurs at 'random' positions throughout the strained volume. The microcracks are oriented mainly along the lines of maximum shear stress.
- Formation of an initial crack: the initial crack starts to grow from the notch root; simultaneously, the microcrack density at some distance from the notch surface increases. This stage of damage evolution corresponds to the beginning of the descending branch on the force-displacement curve. The necking along the shear bands between the microcracks is identified as the mechanism controlling the coalescence of the microcracks.
- Crack growth: the direction of crack growth coincides initially with the shear band formed at the initial stage of deformation. Simultaneously with the growth of the first crack, the density of microcracks inside the specimen increases further. This is followed by the formation of the second large crack at some distance from the notch ground surface.
- Macrocrack coalescence: the large crack which starts from the notch surface joins with the second crack formed in the material due to the coalescence of microcracks far apart from the notch ground surface. The coalescence of these cracks leads to the formation of a large crack and finally to failure of the specimen.

The two macrocracks coalesce, although the microcrack distributions in front of each of them would direct them in different directions. The effect of the interaction of the cracks on their trajectories appears to be more powerful than the effect of the distributed microcracks and shear bands in front of the crack tips for both lamellar and globular alloys.

Although the mechanisms of failure are the same in both alloys, they differ significantly in their overall mechanical response. Due to the more homogeneous distribution of plastic strain in the alloy with the globular microstructure, the coalescence of the microcracks is prolonged to larger total plastic strains and the overall response is significantly more ductile. Further alloy development should therefore aim at the reduction of matrix grain size as well as Si- particle size to achieve a more even distribution of the particles and of the plastic strain.

Acknowledgements

Financial support from BMBF in connection with the COST-512 Program through contract 03K8004, as weal as support from Robert Bosch GmbH and Lasso IngenieuergeseIlschaft, is gratefully acknowledged. The in-situ SEM experiments have been conducted in the Institut für Werkstofftechnik, Technische Universität Bergakademie, Freiberg.

References

[1] Höner KE, Groß J. Bruchverhalten und mechanische Eigenschaften von Aluminium-Silicum-Gußlegierungen in unterschiedlichen Behandlungszuständen. Gießereiforschung 1992;44(4): *146-{iO.*

[2] Gurland J, Plateau J. Trans ASM 1963;56:442-54.
[3] Yeh JW, Liu WP. The cracking mechanism of silicon particles in A357 aluminium alloy. Met Mat Transactions A 1996;27A:3558-63.
[4] Tetelman AS, McEvily Jr AJ. Fracture of structural materials. New York: Wiley & Sons, 1967.
[5] Finkel VM. Physics of fracture. Moscow: Metallurgiya, 1970 (in Russian).
[6] Betekhtin VI, Vladimirov VI. Kinetics of microfractures of crystallic bodies. In: Problems of strength and plas- ticity of solids. Leningrad: Nauka, 1979. p. 142-54.
[7] Lemaitre J. A course on damage mechanics. Berlin: Springer, 1992.
[8] Knott JF. Fundamentals of fracture mechanics. London: Butterworths, 1973.
[9] Thomason PF. A theory for ductile fracture by internal necking of cavities. J Inst of Met 1968;96:360-5.
[10] Seidenfuss M. Untersuchungen zur Beschreibung des Versagenverhaltens mit Hilfe von Schädigungsmodellen am Bespiel des Werkstoffes 20 MnMoNi 55. Dissertation, MPA Stuttgart 1992.
[11] Roberts W, Lehtinen B, Easterling KE. An in situ SEM study of void development around inclusions in steel during plastic deformation. Acta Met Mat 1976;24:745-58.
[12] Hancock JW , Mackenzie AC. On the mechanisms of ductile fracture in high-strength steels subjected to mu1ti- axial stress state. J Mech Phys Solids 1976;24:147-69.
[13] Melin S. Why do cracks avoid each other? Int J Fracture 1983;23:37-45.
[14] Yokobori T. An interdisciplinary approach to fracture and strength of solids. Groningen: Wolter-Noordhoff, 1968.
[15] Ebrahimi F, Seo HK. Ductile crack initiation in steels. Acta Mater 1996;44(2):831-43.
[16] Lippmann N, Steinkopff Th, Schmauder S, Gumbsch P. 3D-finite element modelling of microstructures with the method of multiphase elements. Comp Mat Sci 1997;9:28-35.
[17] Shtremel MA. Strength of alloys. 1. Defects of lattice. Moscow: Metallurgiya, 1982 (in Russian).